XL CILAMCE
IBERO-LATIN AMERICAN CONGRESS ON COMPUTATIONAL METHODS IN ENGINEERING
NOVEMBER 11-14, 2019
Praiamar Natal Hotel & Convention Natal, RN-BRAZIL

INFLUENCE OF AXIAL FORCE ON THE DYNAMIC CHARACTERISTICS OF A BEAM SUPPORTING A ROTATING MACHINE

Flávio José Garzeri
fj.garzeri@gmail.com
Federal University of ABC, Brazil
Bairro Anchieta, Sala 386 - Bloco delta - Campus SBC, 09606-045, São Paulo, Brazil.
Reyolando M.L.R.F. Brasil
reyolando.brasil@ufabc.edu.br
Federal University of ABC, Brazil
Bairro Anchieta, Sala 386 - Bloco delta - Campus SBC, 09606-045, São Paulo, Brazil.

Abstract. We present an experimental study of the effects of geometric nonlinearities on vibrations of rotating machines support structures. Dynamic characteristics of structures depend on their stiffness, damping and mass. The initial stiffness of a structure, computed in its unloaded state, is affected by the applied forces, the so-called geometric stiffness. Compressive forces reduce the stiffness and the frequencies and may lead to buckling, for zero frequencies.

In bases of machines excited by the supported equipment, vibrations may affect the structures but, in general, they may generate damage to the suspended equipment and the quality of the production.

Although machine support structures are, as a rule, very bulky, little affected by geometric stiffness considerations, the tendency of modern structural engineering, especially in aerospace applications, is towards slender members, due to more efficient materials and powerful analysis tools.

Here we study these effects via experimental methods designed to evaluate previous mathematical models. Our model is a metal beam under compression supporting a DC motor. We suppose the original design provided natural frequencies away from the excitation frequency. Nevertheless, the presence of large axial compressive force will reduce the beam stiffness and natural frequencies leading to unexpected, potentially dangerous resonance states.

Experimental imperfections led to observation of interesting phenomena not predicted in our previous theoretical and numerical studies. We also observe, as expected, occurrence of the so called Sommerfeld Effect, when underpowered excitation sources get their rotation regime stuck at resonances.

Keywords: Geometric stiffness, Machine supporting structures, Experimental methods, Sommerfeld effect.

1 Introduction

In this paper, we present an experimental study of the effects of geometric nonlinearities on vibrations of rotating machines support structures. These effects are due to large compressive forces applied to the members of the structure that tend to lower their geometric stiffness and frequencies values. These phenomena tend to be more important in modern structural engineering, especially in aerospace applications, due to the use of slender members, more efficient materials and powerful analysis tools.

Here we study these effects via experimental methods designed to evaluate previous mathematical models. Our model is a metal beam under compression supporting a DC motor. The original design provided for natural frequencies away from the excitation frequency. Nevertheless, the presence of large axial compressive force will reduce the beam stiffness and natural frequencies leading to unexpected, potentially dangerous resonance states.

We also observe, as expected, occurrence of the so called Sommerfeld Effect, when underpowered excitation sources get their rotation regime stuck at resonances.

The model analyzed in the current study is shown on Fig. 1; it is composed of a steel bar under compression that supports a DC motor. The axial compressive force is applied with the aid of a manual hydraulic press, which has been calibrated to allow the measurement of the applied force.

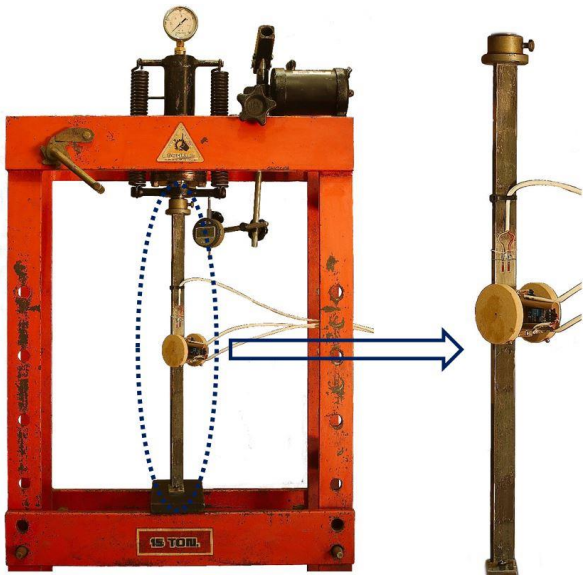

Figure 1. Model installed in a manual hydraulic press.

The effect of the axial load on the resonant frequency of the model was verified experimentally in a static test; increasing axial loads were consecutively applied while the resonance frequency was measured by a simple impact test. With the behavior of the first frequency determined by this test, a second experiment was performed. The model was axially compressed and the motor was accelerated progressively to a rotational frequency above the corresponding natural frequency. As expected, the resonance of the model occurred before that one measured with zero loading and the Sommerfeld effect was observed.

This model has already been analyzed mathematically and numerically by Brasil [1]. A brief mathematical analysis, based on this work, is presented allowing the comparison of the experimental results with theoretical data for two distinct boundary conditions. Such comparison showed that experimental imperfections led to observation of interesting phenomena not predicted by theoretical and numerical studies mentioned above.

2 Mathematical model

The structure shown on Fig. 1 can be represented by a simply supported beam with linear elasticity module *E*, length *L* (see Fig.2), and constant rectangular cross section with *W* width and *t* thickness resulting a moment of inertia *I*. To complete the model, an electric motor is attached to its center through a rigid support. The total mass of the motor and its support is M_c. In order to represent the compressive force provided by the hydraulic press, an axial force *P* is acting on the axially free support *B*.

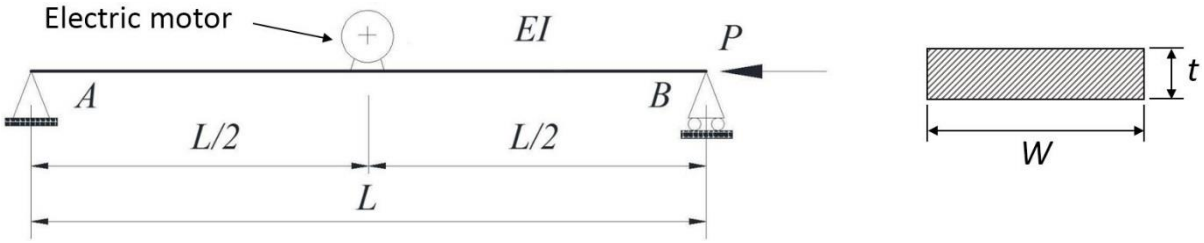

Figure 2: Beam model and its cross section.

The mathematical model shown on Fig. 2 is, of course, continuous, with infinite degrees of freedom. A simple SDOF (Single-Degree-Of-Freedom) analysis can be performed, if it is assumed that its motion can be approximately represented by a single flexure deflection pattern times the displacements of the central point of the beam. As the main purpose of the analysis is to determine the first natural frequency, the first natural mode shape is assumed as the flexure deflection pattern ($\phi(x)$), usually called a shape function.

Figure 3 shows the analytical model and its equivalent single degree of freedom system for the displacement of the middle point, with first natural frequency *f*. The vertical displacement of the middle point with time *t* is the generalized coordinate *q(t)* and the vertical displacement of any point of the beam, *v(x,t)*, is given by Eq. 1. In order to keep the model simple, the eccentricity between the axis of the motor and the beam is ignored and the motor inertia and its support mass were modeled as a lumped mass, M_c, in the center of the beam.

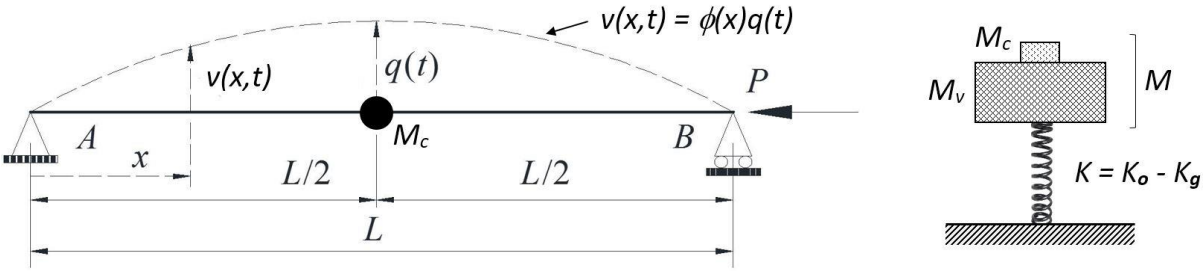

Figure 3: Analytical model and its equivalent mass/spring system.

$$v(x,t) = \phi(x).q(t)\,. \tag{1}$$

The generalized properties of the beam are calculated by Eq. 2 to 4, considering m_v as the beam mass per unit length. The properties of the equivalent single of freedom system are calculated by Eqs. 5 to 7. The complete deduction of these expressions, assuming Euler-Bernoulli hypothesis for the beam and the principle of virtual work, is found in Brasil [1] and Clough and Penzien [2].

$$K_o = \int_0^L EI\left(\frac{d^2\,\phi(x)}{dx^2}\right)^2 dx\,. \tag{2}$$

$$K_g = P\int_0^L EI\left(\frac{d\,\phi(x)}{dx}\right)^2 dx\,. \tag{3}$$

$$M_v = \int_0^L m_v\phi(x)^2 dx\,. \tag{4}$$

$$M = M_v + M_c\,. \tag{5}$$

$$K = K_o - K_g\,. \tag{6}$$

$$f = \frac{1}{2\pi}\sqrt{\frac{K}{M}}\,. \tag{7}$$

If we adopt the shape function cited in Blevins [3] for the first natural vibration mode of a simply supported beam,

$$\phi(x) = sin\left(\frac{\pi x}{L}\right)\,. \tag{8}$$

we can calculate the properties as mentioned above, finding the following expressions:

$$K_o = \frac{\pi^4 EI}{2L^3}\,. \tag{9}$$

$$K_g = \frac{P\pi^2}{2L}\,. \tag{10}$$

$$M_v = \frac{m_v L}{2}\,. \tag{11}$$

$$f = \frac{1}{2}\sqrt[2]{\frac{\pi^2 EI - PL^2}{L^3(Lm_v + 2M_c)}}\,. \tag{12}$$

It is important to mention that the accuracy of the frequency calculated by this method (equivalent SDOF analysis of a continuous system) depends on the shape function $\phi(x)$ considered to represent the vibration mode. $\phi(x)$ adopted (Eq.8) is the exact 1st mode shape function for a pined-pined beam.

Similarly, adopting the following shape function:

$$\phi(x) = \gamma_1\left(cosh\left(\frac{\lambda x}{L}\right) - cos\left(\frac{\lambda x}{L}\right)\right) - \gamma_2\left(sinh\left(\frac{\lambda x}{L}\right) - sin\left(\frac{\lambda x}{L}\right)\right).$$

$$where\ \begin{cases}\gamma_1 = 0.629664937\\ \gamma_2 = 0.618647186\\ \lambda = 4.73004074\end{cases} \tag{13}$$

which is suitable for the first natural vibration mode of a clamped-clamped beam, the first natural frequency, f_{cc}, is found to be:

$$f_{cc} = 3.561\sqrt[2]{\frac{EI - 0.02458L^2P}{L^3(LM_v + 2.522M_c)}}\,. \tag{14}$$

3 Experimental Evaluation

As mentioned in the Introduction, the steel bar was subjected to compression loads in a manual hydraulic press. During the test, load amplitude, bending moment near the center of the column, displacements of the hydraulic piston and the natural frequency of the first mode were measured. As also mentioned in item 1, experiments were performed with the electric motor running and other variables were measured, namely: power consumption, supply voltage, vibration and strain amplitudes near the center of the beam. Next we describe characteristics of the bar, electric motor and electronic devices, specially constructed to allow these measurements with reasonable accuracy.

3.1 Steel bar

The bar used in the tests is made of low carbon steel. It was prepared [4] to receive strain-gauges near its center, in order to measure bending moments during the quasi static tests (the ones performed to measure the behavior of the first natural frequency in relation to axial load). The material and geometric characteristics of the bar are shown on Table1.

Table1. Material and geometric characteristics of the bar.

Characteristic	Nomenclature	Value	Unit
Mass	*M*	0.797	Kg
Lumped Mass	*Mc*	0.2253	Kg
Modulus of elasticity	*E*	1.99×10^{11}	N/m^2
Average Width	*W*	0.0312	m
Average Thickness	*t*	0.00628	m
Length	*L*	0.526	m

Figure 4 shows a support made of rigid plastic (PVC), which was fixed in the middle of the bar to allow the installation of a small direct current (DC) electric motor. The figure also show the flywheels, electric motor and strain gauges, which are discussed later.

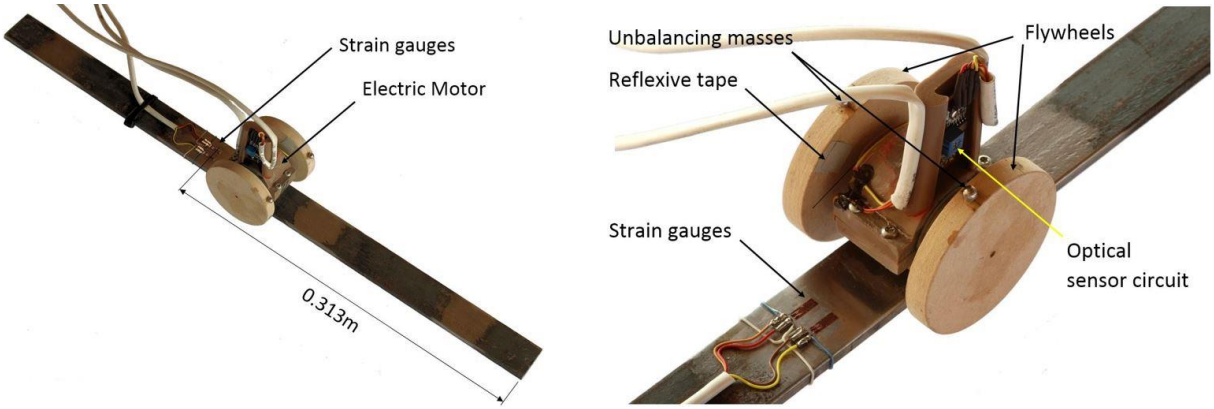

Figure 4. Bar with plastic support for the electric motor and strain-gauges.

In order to simulate simply supported ends, three solutions were tested: partially embedded spheres, simply filed and sharp pins as terminations (see Fig. 5).

Figure 5. Types of bar termination: embedded sphere, simply filed, embedded pin.

3.2 Electric Motor and flywheels

A small carbon brush electric motor, DC powered, made by Mabuchi (RS-385-SH model) was chosen to excite the bar. As the motor had double output shaft, two unbalanced flywheels were installed, one at each side of the engine, and were positioned in such a way that only an unbalancing force (no moments) resulted from their rotation. The flywheels were made of MDF and the total unbalancing mass was 0.008kg@0.0336m. An electrolytic capacitor of 5000μF was connect in parallel with the motor, to minimize voltage ripple.

3.3 Wattmeter

In order to measure power consumption by the electric motor, a low cost wattmeter with proportional DC output voltage has been built. Figure 6 shows a schematic diagram of the device with specially made circuits (2nd order low pass filter [5] and low ripple power supply) and commercial parts, made by Texas Instruments [6] and Microchip Technology [7].

The high precision, low ripple power source was crucial to assure accuracy in the digital to analog conversation, which was verified to be less than 1% during the wattmeter calibration.

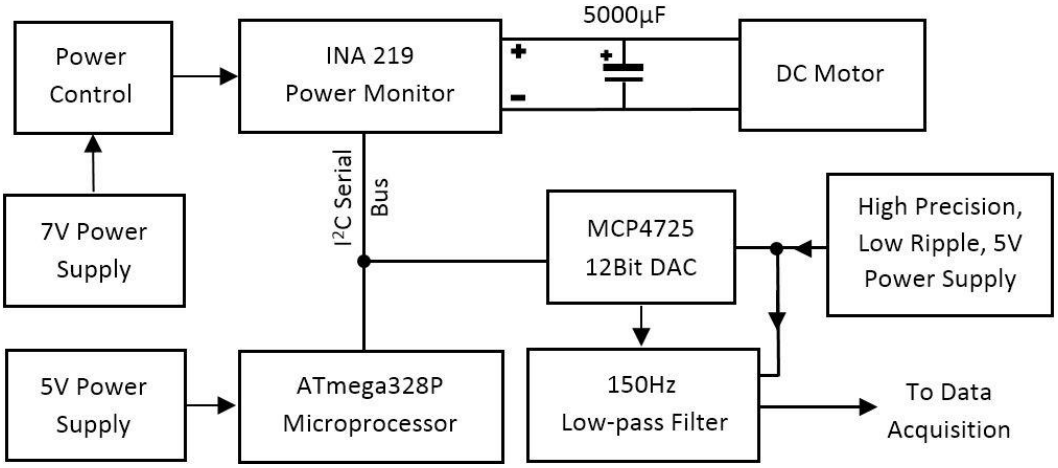

Figure 6: Schematic diagram of the wattmeter.

3.4 Tachometer

A low-cost tachometer has been specially built to accurately measure small variations in motor speed during acceleration through the structural resonance. Figure 7 shows the schematic diagram of the device with an optical sensor made by Vishay [8] and other commercial components already mentioned in item 3.3.

It has been found that such a tachometer can accurately measure velocity variations of up to 100Hz and its accuracy is better than 0.3% in the measurement range from 1200rpm to 3000 rpm.

3.5 Bending moment measurement device

Four 120Ω, 5mm long strain-gauges, were glued to the surface of the bar at 0.313m from one of its ends (see Fig. 8). In order to measure only bending moments, they were connected in a specific Wheatstone bridge arrangement, as described by Dally [9].

The Wheatstone bridge was connected to a specific 24-bit Analog-Digital Converter (HX711, by AVIA[10]), configured to provide 5V (DC) power supply, which minimized power dissipation by the strain gauges, thereby increasing measurement stability as suggested by Micro Measurements[11]. The ADC was connected to a microprocessor to show, through a liquid crystal display (LCD), deformation values during measurements of the variation of the 1st natural frequency of the bar with respect to compression load. During dynamic measurements - bar excited by the electric motor – the Wheatstone bridge was connected to a data acquisition system, which also supplied energy to the strain-gauges.

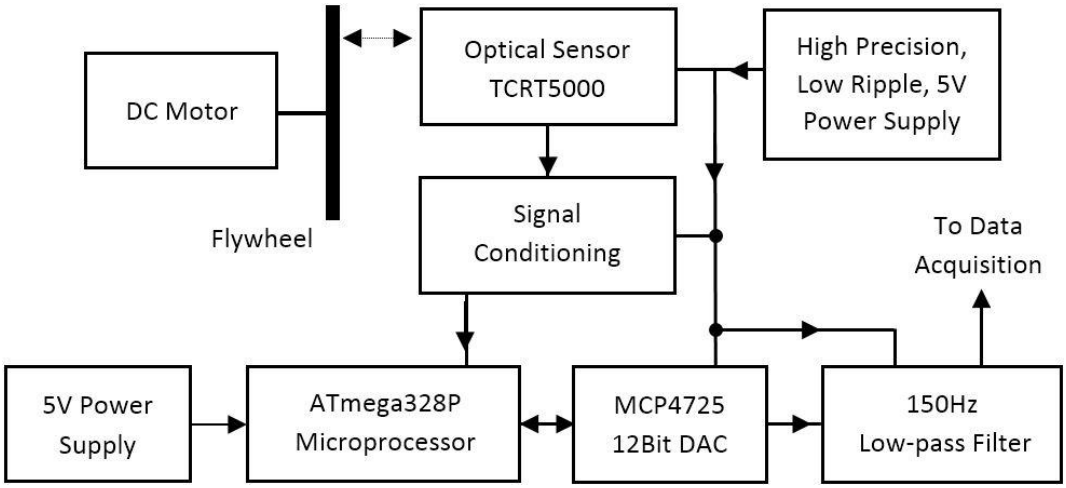

Figure 7. Schematic diagram of the tachometer.

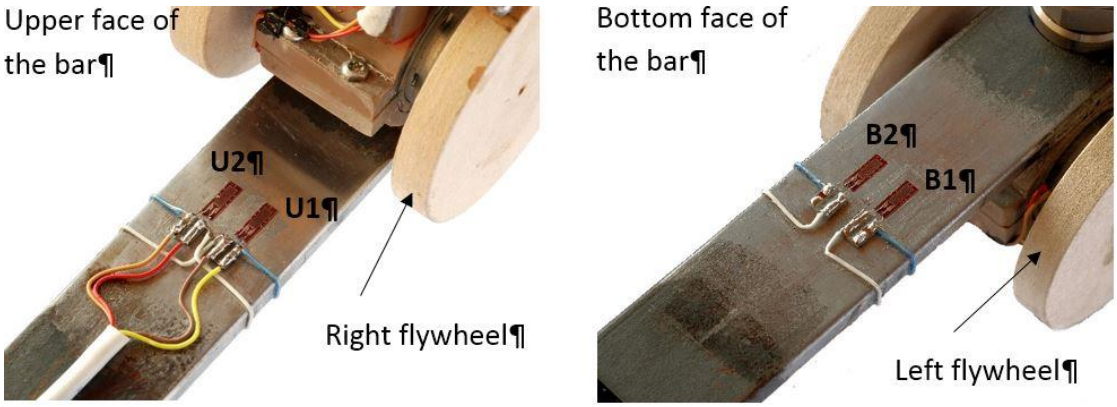

Figure 8. Strain-gauges on bar surface.

By fixing the bar on the horizontal position through one of its ends and applying known weights at the other end (cantilever configuration), it was possible to calibrate the strain apparatus in terms of bending moments.

3.6 Power supply control strategy

In order to drive the electric motor as smoothly and repetitively as possible during the measurements, an electronic circuit was built. By using an operational amplifier and a power transistor, the DC voltage supply to the motor was controlled by a small AC signal, delivered by an electronic function generator. The generator was setup to provide a ramp signal, whose period was adjusted to allow a slow passing through the bar resonance.

3.7 Vibration amplitudes and frequency measurements

Vibration amplitudes in the middle of the bar were measured by a piezo accelerometer connected to a signal amplifier. The AC output of the amplifier was either connected to a data acquisition or oscilloscope with FFT capability, depending on the kind of measurement (see item 3.8).

3.8 Data acquisition

The variation of the 1st natural frequency of the bar with respect to compression load was

measured with an FFT oscilloscope connected to an accelerometer (item 3.7). Compression load was set manually, using a hydraulic press and then, the bar was hit by an impact hammer in the middle of the bar, in order to excite its first natural mode.

During dynamic tests with the motor on, the following variables were measured: vibration and deformation amplitudes at 0.25m and 0.313m from the bar end, respectively, rotation and power consumption of the motor, voltage supplied to the motor. All measurements were acquired by a DC, 8-data-channel acquisition system. The acquisition data sampling was set to 8 kHz, in order to allow properly graph display of transients.

4 Experimental results

The behavior of the first natural frequency and bending moment (close to the center of the bar) regarding the axial force is shown on Fig. 9. The theoretical behavior of this frequency, expressed by Eq. 12, is also plotted to allow comparisons with data obtained with the three types of terminations shown on Fig. 5. For reference only, the theoretical buckling force for a beam with simply supported boundary conditions is also shown on the right side of the graph. Figure 10 shows the bending moments near the center of the bar during the tests. It is important to mention that curve markers on both figures are actually data points.

Figure 11 shows the vibration amplitude close to the center of the bar, while Figs. 12 and 13 show the motor rotation, power consumption and voltage supply during a speed up through the resonance of the system. The axial load was kept constant at 3350N, approximately, during the data acquisition. The bar ends used in this test were those with partially embedded spheres.

As mentioned in item 3.8, the deformation at 0.31m from the bar end during motor acceleration was also acquired and is shown on Fig. 14. The engine speed is also plotted for ease of comparison with the data shown on Fig. 11.

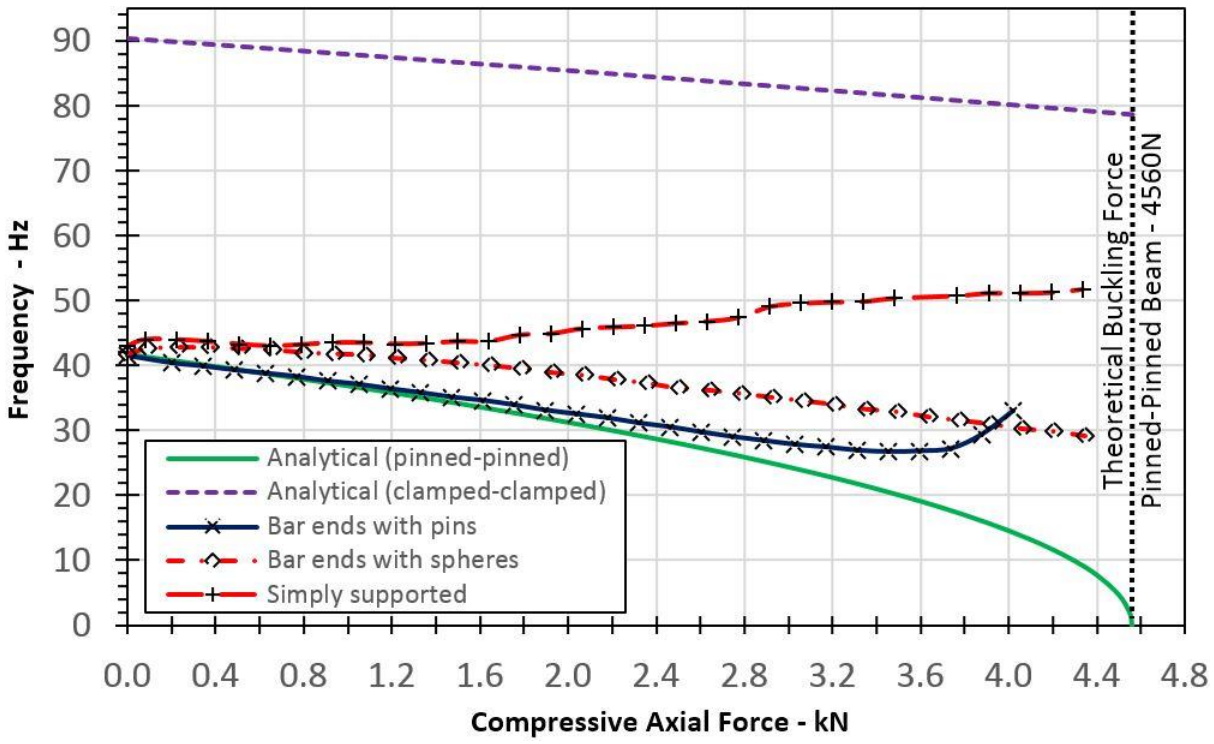

Figure 9: Influence of the axial force on the 1st natural frequency and bending moment.

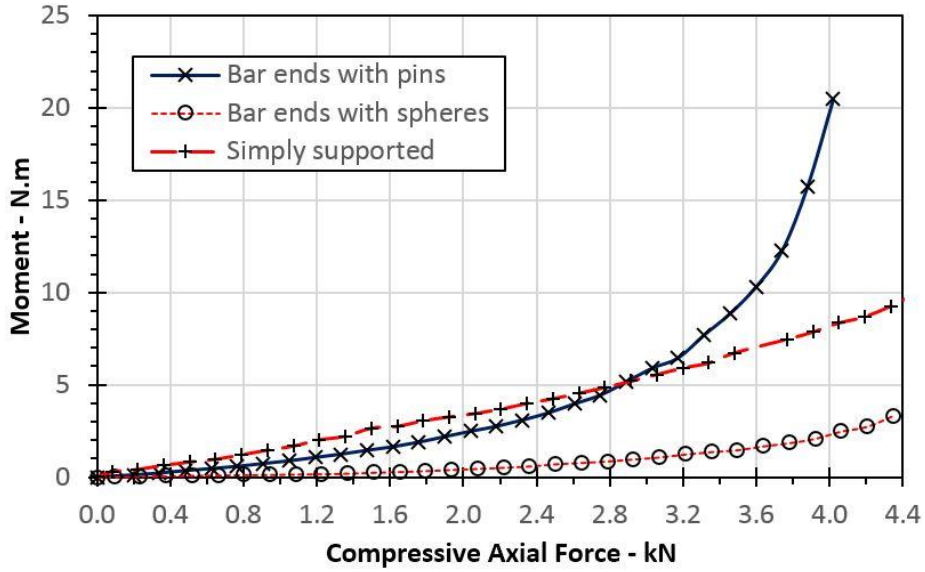

Figure 10: Bending moments at 0.313m from the bar end during the measurements shown on Fig.8.

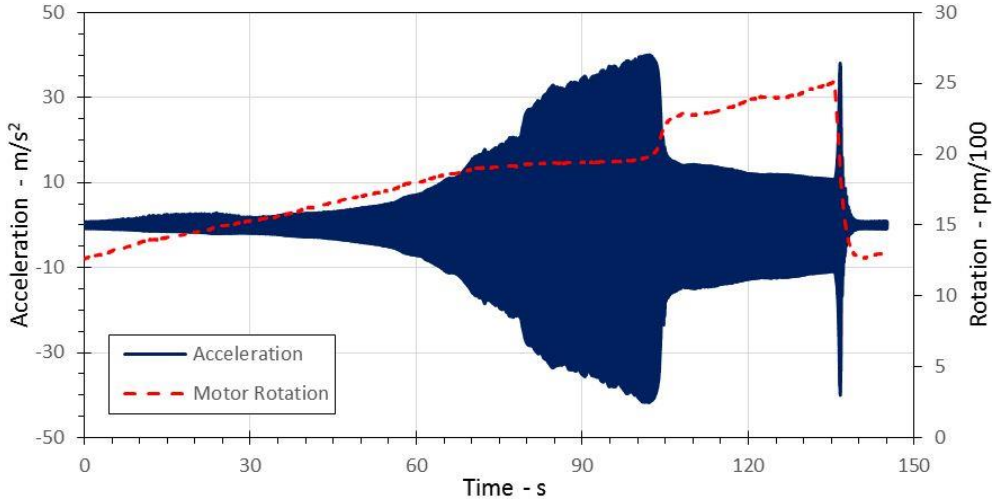

Figure 11: Acceleration close to the center of the bar through structural resonance

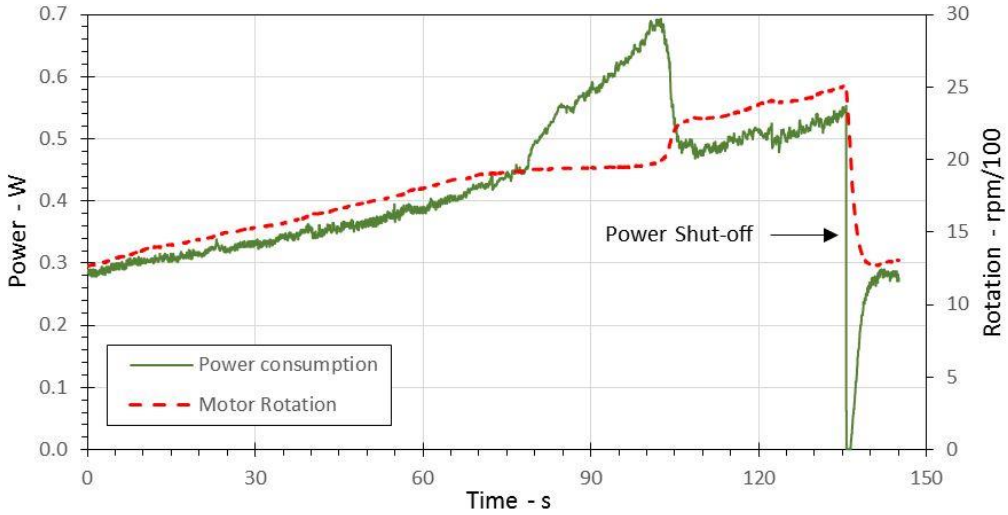

Figure 12: Motor rotation and power consumption through structural resonance.

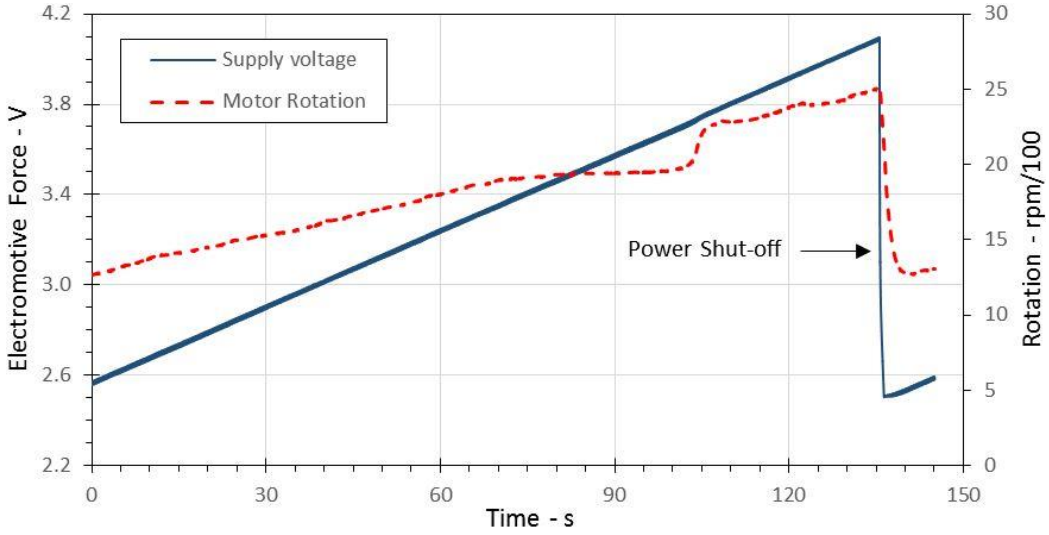

Figure 13: Motor rotation and power supply voltage through structural resonance.

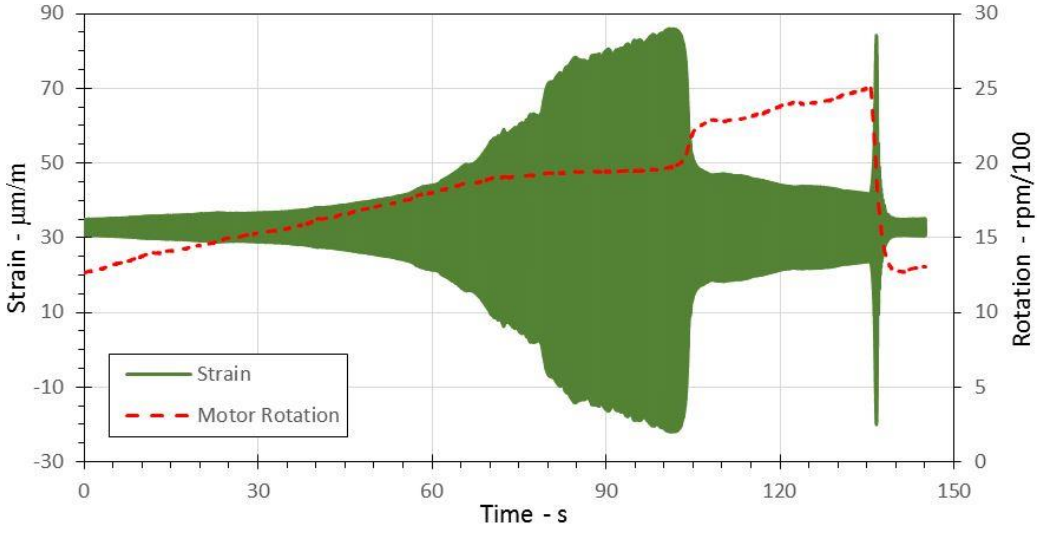

Figure 14: Strain close to the center of the bar through structural resonance.

5 Comments and conclusions

Considering the results shown on Fig. 9, it is clear the influence of the axial force on the dynamic characteristics of the analyzed beam: the higher the axial force, the lower its first natural frequency.

However, the observed behavior of the 1st natural frequency is not fully predicted by the theory presented in item 2. After a certain magnitude of the axial force, its decreasing rate changes and, when the force reaches a critical value, the initial tendency reverses: the magnitude of the natural frequency goes up quickly with the increase of the axial force.

An explanation for this unpredictable behavior, opposite to the theory presented, is that the beam assumes a curved shape after a certain magnitude of the axial force, contrary to the initial hypothesis of the mathematical model adopted of remaining straight. Therefore, the shape function initially adopted, $\phi(x)$, is no longer adequate, causing significant errors. The bending moment near the center of the beam, which can be considered as an indicator of the beam curvature, was measured during the tests and its behavior corroborates this explanation.

Another factor that contributes so that the adopted model is not fully representative of the system tested is the assumption of ideal pinned bar ends. An ideal pinned end is free to rotate and the contact between support surface and the pin can be represented by a single point. However, that is not verified

in a normal test condition. Due to constructive mechanical limits and the elasticities of the pin and surface support materials, the contact between both, under compressive load, becomes an area. Besides, depending on the compressive force magnitude applied to the pin, the frictional forces present on the contact surface can impose considerable restrictions on its rotation. In addition, it is experimentally observed that the larger the contact area the greater the reaction to the rotations. So, in real experimental conditions, pinned ends can react to rotations and this reaction will depend on, among several factors, the axial forces, size of the contact surface and friction coefficient between the materials involved.

In order to avoid slippage of the bar during the experiments, the support surface was prepared; in the sphere termination, a concave hole with diameter about 4mm was machined, allowing the sphere to get embedded in the support surface. In the pinned termination, a hole about 1mm was drilled. Figure 15 show both terminations in test configuration and Fig. 16, the exploded view of them, highlighting contact surfaces. Considering the sizes of the surface contacts in the support surface, it is expected that the embedded sphere termination is stiffer than the pinned one in terms of rotation of the bar end.

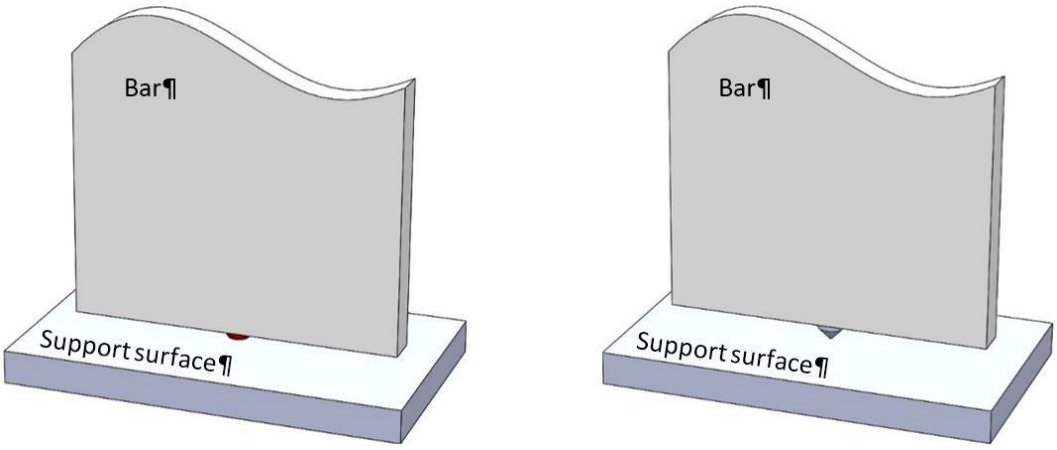

Figure 15: Embedded pin and sphere terminations at test condition.

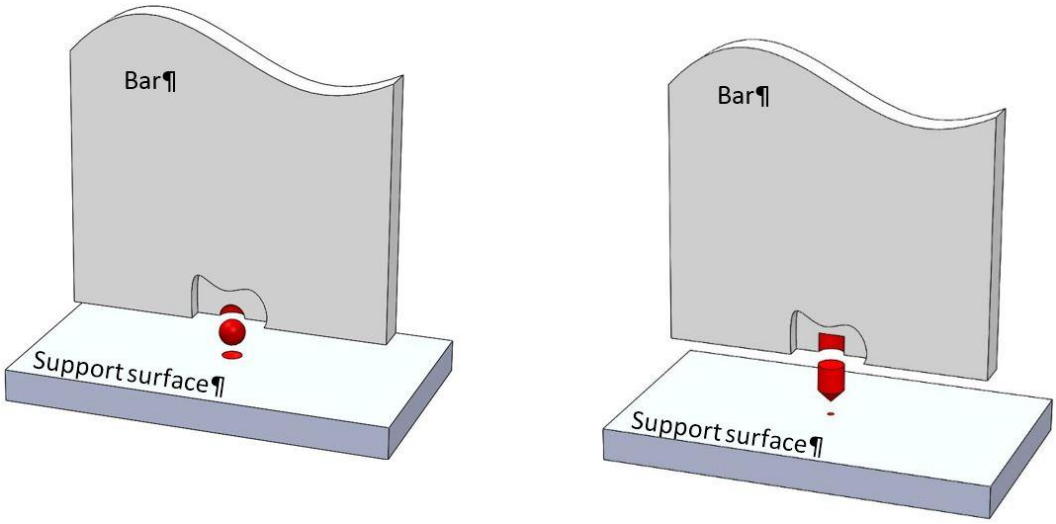

Figure 16: Contact surface differences between the embedded pin and sphere terminations.

The most critical termination tested, in terms of nonideal behavior, was the simply cut and filed bar end. Due to its irregular surface, a full contact with the support surface was not achieved. Besides, when axial force was applied, its surface deformed, allowing other points to get in contact with the support surface, changing the boundary condition during the experiment, Therefore, considering the

above explanation, this type of termination became increasingly stiff as the applied axial force was increased.

Figure 17 shows the contact points - in black - of the simply cut and filed bar end with the support surface under two loading conditions: 500N (left pictures) and 4kN (right picture), approximately (dashed lines indicate the perimeter of the surface of the bar end). These contact patterns were determined experimentally and corroborate the explanation of the increase of the contact area with the axial load elevation.

Figure 17: Contact patterns of the simply cut and filed end under two load conditions: 500N and 4kN.

It is interesting to compare the 1st natural frequency measurements, considering the three types of terminations (Fig. 5), with the theoretical behavior of this frequency considering clamped-clamped bar ends (Eq.14). This comparison can be seen on Fig. 9. Notice how the data obtained with the simply filed ends tend toward the theoretical prediction with clamped ends the greater the axial force.

Considering the data acquired with the electric motor turned on (Fig. 11), it is important to notice that the rotational acceleration of the motor decreases close to the resonance frequency of the system (33.3Hz or 1998rpm for the test conditions), although the increasing voltage rate is kept constant by the power control (Fig. 13). Besides, the closer the motor rotation approaches the natural frequency of the system, the more power the motor requires to increase its speed (Fig. 12). If the motor had limited power, it would not go through the resonance, getting stuck at a certain speed.

The motor needed about 55% more power to go through the system resonance. The energy consumed in this process was consumed by the motor (in internal losses and to increase its speed) and the rest was transferred to the structure through the unbalancing masses attached to the flywheels. Part of the energy transferred to the structure increased its vibration amplitude, and another part consumed by the structural damping. After going through the resonance, the motor rotation increased rapidly. This phenomenon (rotation jump) is known as Sommerfeld effect and has been analyzed by Brasil [12], Balthazar and Tusset and Brazil [13], Balthazar, Brasil and Felix [14].

It is also important to comment about strain and vibration amplitudes (Fig. 8 and 9). The strain and vibration amplitudes behaviors are very similar. The difference resides on the asymmetrical shape of the strain curve in relation to *x* axis. The strain curve is above the *x* axis by 33με approximately, due to the shape of the bar under the axial load of 3350N. This load was chosen because it allowed a considerable reduction of the natural frequency, compared to the unloaded bar, and for becoming evident the effects of the imperfections inherent to the test (bending moments close to the center of the bar).

Last, it is necessary to emphasize the importance of considering the geometric stiffness in structures that support rotating machines or other equipment capable of exciting it. As it was verified, the natural frequencies can be very different from those calculated for the unloaded structure. Thus, it is possible that a structure designed as safe and stable may exhibit considerable vibration amplitudes that may cause structural damage or problems related to production quality, efficiency etc. The effects of geometric nonlinearity on the dynamic behavior of structural resonance has been analyzed by Brasil and Wahrhaftig [15] and Brasil and Balthazar [16, 17].

6 Acknowledgements

The authors acknowledge support by FAPESP, Fundação de Apoio à Pesquisa do Estado de São Paulo (Grant 2017/06076-0**).**

We would also like to express our appreciation to André Cóstola (General Motors of Brazil), for the suggestions about the power controller circuit, which was used during the experiments.

7 References

[1] BRASIL, Reyolando M. L. R. F – "Theoretical and experimental analysis of nonlinear geometric stiffness effects on machine support structures" In: 16th Pan-American Congress of Applied Mechanics (PACAM). Ann Arbor, MI, American Academy of Mechanics, 2019. v.1. p.65-70.

[2] CLOUGH, R.W.; PENZIEN, J. – "Dynamics of Structures" In: - Generalized single-degree-of-freedom systems. 2. ed. McGraw-Hill, 1993, p. 140-143. /International Edition/.

[3] BLEVINS, R. D. - "Formulas for natural frequency and mode shape" In: - Straight beans. Krieger Publishing, Malabar, Florida, 2001, p. 107-118.

[4] MICRO MEASUREMENTS – Instruction bulletin B-129-8: surface preparation for strain gage bonding. rev. 08-07. Wendell, North Carolina, 2014.

[5] LANCASTER, D. – "Active-filter cookbook" In: - low-pass filter circuits. Carmel, Indiana, 1975, p. 118-138.

[6] TEXAS INSTRUMENTS – INA219: zero-drift, bidirectional current/power monitor with I2C interface. Dallas, Texas, 2008.

[7] MICROCHIP TECHNOLOGY - MCP4725: 12-bit digital-to-analog converter with EEPROM memory in SOT-23. Chandler, Arizona, 2009.

[8] VISHAY SEMICONDUCTORS – TCRT5000: reflective optical sensor with transistor output. rev. 1.7. Malvern, Pennsylvania, 2009.

[9] DALLY, J. W. & RILEY, William F – "Experimental Stress Analysis" In: - strain-gauge circuits. 3 ed. McGraw-Hill, 1991, p. 223-228.

[10] AVIA SEMICONDUCTOR - HX711: 24-bit analog-to-digital converter (ADC) for weigh scales. Xiamen, China, 2009.

[11] MICRO MEASUREMENTS – Tech note TN-502-1: optimizing strain-gauge excitation levels. Wendell, North Carolina, 2014.

[12] BRASIL, Reyolando M. L. R. F. – "A non-linear dynamic model of a non-ideal motor support structure" In: XXXIV Ibero-Latin Congress on Computational Methods in Engineering (CILAMCE 2018). Compiegne, France, 2018. v.1. p.10-.

[13] BALTHAZAR, José M.; TUSSET, Angelo M.; BRASIL, Reyolando M. L. R. F.; FELIX, Jorge L. P.; ROCHA, Rodrigo T.; JANZEN, Frederic C.; NABARRETE, Airton; OLIVEIRA, Clivaldo - An overview on the appearance of the Sommerfeld effect and saturation phenomenon in non-ideal vibrating systems (NIS) in macro and MEMS scales. *Nonlinear Dynamics*, v.91, p.1-12, 2018.

[14] BALTHAZAR, José M.; BRASIL, Reyolando M. L. R. F.; FELIX, Jorge L Palacios – "An overview of nonlinear dynamics of electromechanical engineering systems excited by small motors" In: COBEM 2015. Rio de Janeiro, Brazil, 2015. v.1, p.40-.

[15] BRASIL, Reyolando M. L. R. F.; WAHRHAFTIG, Alexandre de Macedo – "Experimental evaluation of the effect of geometric nonlinearities on structural resonances" In: 7th International Conference on Experimental Vibration Analysis for Civil Engineering Structures (EVACES 2017). San Diego, CA, University of California, 2017. v.1, p.12-.

[16] BRASIL, Reyolando M. L. R. F.; BALTHAZAR, José Manoel – "On the effect of geometric nonlinearity on resonance in a machine foundation" In: 11th World Congress on Computational Mechanics (WCCM XI). Barcelona, Spain, International Center of Numerical Methods in Engineering, 2014. v.1, p.164 - .

[17] BRASIL, Reyolando M. L. R. F.; BALTHAZAR, José Manoel – "The effect of geometric nonlinearity on the dynamic behavior of a machine suspension structure" In: 10th International Conference on Mathematical Problems in Engineering, Aerospace and Sciences (ICNPAA 2014). Narvik, Norway, AIAA, American Institute of Aeronautics and Astronautics, 2014. v.1, p.17 - .